Hindawi
Geofluids
Volume 2022, Article ID 1139232, 18 pages
https://doi.org/10.1155/2022/1139232

Research Article

Characteristics of Pore-Throat in Tight Sandstones of the Jurassic Ahe Formation in the Northern Tarim Basin

Tong Lin,[1] Cong Tan,[1] Xing Zhang,[2] Lei Zhao,[3] Hongxing Wei,[2] Lan Wang,[1] Xin Nie,[4] and Xu Zeng[1]

[1]*Research Institute of Petroleum Exploration & Development, PetroChina, Beijing 100083, China*
[2]*Research Institute of Exploration and Development, Tarim Oilfield Company, PetroChina, Korla, Xinjiang 834000, China*
[3]*Qingdao Geo-Engineering Surveying Institute (Qingdao Geological Exploration and Development Bureau), Qingdao 266000, China*
[4]*Key Laboratory of Exploration Technologies for Oil and Gas Resources, Yangtze University, Wuhan, Hubei 430100, China*

Correspondence should be addressed to Cong Tan; 340330888@qq.com

Received 30 August 2021; Revised 30 November 2021; Accepted 16 December 2021; Published 28 January 2022

Academic Editor: Chenhao Sun

In order to clarify the characteristics of pore-throat in tight sandstone reservoirs in the Dibei area of the Kuqa Depression in the Tarim Basin (Northwest China) and to make clear its impact on reservoir quality and productivity, microscopic observation and quantitative analysis of 310 tight sandstones in the Kuqa Depression are carried out by using various methods. Microscopic observation shows that the shapes of the pores are flat, oval, and long-narrow. A great number of throats connect the nanoscale pores in the form of a network. Quantitative analyses including RCMP (rate-controlled mercury penetration), HPMI (high-pressure mercury injection), NA (nitrogen adsorption), and routine and stress-dependent core analysis show that the peak of pores radius ranges from 125 μm to 150 μm, and the throat radius is in the range of 1 μm-4 μm. The throat space accounts for about 2/3 of the total space of the tight sandstones, which is the major storage space for natural gas. The space shape has a great influence on the reservoir seepage capacity, particularly under the condition of overburden pressure. The pores with throat radius greater than 300 nm have free fluid, and they contribute more than 98% of the reservoir permeability. The pore spaces with throat radius among 300 nm-52 nm can release fluids by reservoir stimulation. The pore-throats with radius < 52 nm cannot release the irreducible hydrocarbon fluids. In addition, formation pressure is easy to destroy tight sandstone reservoir. The research results will provide insights into the efficient recovery of natural gas in tight sandstones.

1. Introduction

Porosity and permeability are two major parameters for evaluating reservoir quality, and there is usually a good linear correlation between them [1–4]. However, in unconventional reservoirs (such as tight sandstone reservoir, shale reservoir, tight limestone, and volcanic reservoir), the correlation between porosity and permeability is not as close as that in conventional reservoirs [5–7]. More and more researchers have realized that the throat in the reservoir is the key factor to affect the seepage capacity of the reservoir, and it also determines the oil and gas production capacity of the reservoir [8–12]. Nelson [13] has introduced the distribution of throat sizes in different types of rocks. Based on his measured data, it is believed that changes in throat size have the most significant impact on reservoir permeability. If the throat size changes by one order of magnitude, the permeability value will change by more than two orders of magnitude, so that throat is a critical parameter to evaluate reservoir quality. Pittman established a method to evaluate the quality of low-permeability reservoir by throat size as early as 1989 and achieved good results [14]. Reservoir quality evaluation with throat as a parameter, especially the evaluation of tight sandstone reservoirs, is relatively scientific and effective, and a lot of achievements have been made in related research ([14]; Lu et al., 1997; [15]; Wen et al., 2005; [16]; Li et al., 2007; [17, 18]; Li et al., 2012; [19]).

For the tight sandstone reservoirs, the size, distribution, and morphology of pore-throat are closely related to reservoir quality [20–22]. When Deng et al. [23] carried out

sandstone reservoir classification, they clearly pointed out that the long and narrow fractures between grains and quartz secondary enlarged edges have obvious control effect on reservoir quality and oil and gas production, and this type of fracture is very sensitive to stress.

The tight sandstone gas-bearing area of the Jurassic Ahe Formation in the eastern Kuqa Depression, Tarim Basin, located close to the source of China's "West to East Gas Transmission", is an important succession field of natural gas supply in the future. However, the understanding of tight sandstone gas reservoir in the Ahe Formation is still very limited, so that many wells have damaged the reservoir in the process of drilling or reservoir stimulation, which has seriously affected the tight gas productivity in this area. Therefore, it is necessary to study the microscopic characteristics of tight reservoirs in the Ahe Formation.

The main purpose of this study is to characterize the pore-throat of the tight sandstone reservoirs in the Dibei area of the Kuqa Depression in the Tarim Basin (Northwest China) and decipher the relationship between reserves and productivity with throat based on multiproxy of quantitative measurement. It is hoped to provide some enlightenment for the effective exploitation of natural gas in tight sandstone.

2. Geological Setting

2.1. Tectonic Setting. The Kuqa Depression is situated at the north edge of the Tarim Basin (Figure 1) [24]. It is a foreland depression which was formed in the subduction and collision of the Tarim plate to the Tianshan Mountain in the Triassic [25–28]. Influenced by the shallow layers of the South Tianshan orogenic belt thrusting southward, a series of E-W direction thrust faults are developed in the Kuqa foreland, thrusting towards the basin [29]. The Dibei area is located in the middle section of the Yiqikelike fault belt, the north margin of the Yangxia sag in the east of Kuqa Depression, with the characteristics of linear anticlines, faulted anticlines, and faulted nose structures (Figure 2) [24]. The fault belts began to thrust at the Late Miocene and continued until now. The tectonic movements in the Jurassic and Early Cretaceous led to a transformation from fault propagation folds to large-scale fault-bend anticlines in the Dibei area [30]. Compressional uplift and erosion during the Late Cretaceous resulted in the formation of current structural and sedimentary features in the study area [31–33].

2.2. Features of Tight Sandstone Gas Reservoir. More than ten wells have drilled the tight sandstone reservoir in the Ahe Formation (J_1a) of the Lower Jurassic in the study area. Among them, Well Yn2 has obtained high-yield industrial gas flow, Well Yn5 is a low-yield gas well, and other wells have different levels of oil and gas, indicating that Dibei is an important area for oil and gas accumulation.

The reservoir of the Ahe Formation is buried in the depth between 4500 and 5000 m and consists of channel sandstone of the braided river delta plain. Laterally, the sandstones are continually distributed with an average thickness of 180-230 m. Vertically, the Ahe Formation can be divided into several fining-upward sedimentary cycles. From bottom to top, conglomeratic sandstones of braided river channel in flood plain facies are gradually transformed to siltstones and mudstones of flood plain facies. Due to the erosion of the lateral migration of the channel sandstone in the floodplain facies, the top silt is generally absent, and the lower part of the channel is retained, forming several sets of incomplete cycles. The physical properties of the reservoir are positively correlated with the sedimentary cycle; the porosity and permeability of the coarse sandstone at the cycle bottom are apparently better than those of the fine sandstone at the top.

The sandstones of the Ahe Formation deposited under the control of the provenance and sedimentary facies belts of the southern Tianshan Mountains in the north [37–39]. The lithology is feldspar lithic sandstone or lithic sandstone, with moderate particle sorting properties, and mainly composed of the coarse sandstone, conglomeratic sandstone, and medium sandstone. The sandstone is compact and has almost no macroscopic dissolved pores in cores, but dissolved fractures and tectonic fractures are observed in several wells.

3. Samples and Methods

56 samples of 7 wells were collected from the tight sandstone of the Ahe Formation in the study area (Figure 1). All the samples are from the depth of 4000-5000 m except for the samples from Well Mn1 in the eastern part of the study area are at the depth of 965-1150 m. The length of the cylindrical core samples is 5-12 cm, and the cross-sectional diameter is 2.5 cm. Series of matching analyses were carried out for the 56 samples (Table 1), including thin section (CTS), scanning electron microscope (SEM), confocal laser scanning microscope (CLSM), rate-controlled mercury penetration (RCMP), high-pressure mercury injection (HPMI), nitrogen adsorption (NA), porosity and permeability analysis under normal pressures (PPNP), and overburden pressures (PPOP).

Before grinding thin sections, the samples were injected with epoxy resin of the mixture of ferrocyanide and alizarin red under vacuum pressure, so that the pore space of sandstone reservoir can be clearly observed under the single polarized light microscope, and the characteristics and content of calcite cement can be easily identified. Similarly, when grinding laser confocal thin sections, a special enhanced fluorescent agent was injected into the samples; therefore, the subtle cracks which cannot be observed in casting sections can be identified by the intense fluorescence under laser excitation.

3.1. RCMP. RCMP (rate-controlled mercury penetration) experiment was conducted on the ASPE-730 model equipment from American Coretest Systems Company. Before analysis, the plunger samples were washed and dried, and the porosity and permeability were measured. Then, the samples were immersed in mercury solution after vacuum, the interfacial tension and contact angle were kept unchanged, and mercury was injected into the core at a very low constant speed (0.00005 ml/min). When the pressure reached at 900 psi (about 6.2 MPa), the experiment ended. During the experiment, real-time monitoring and automatic

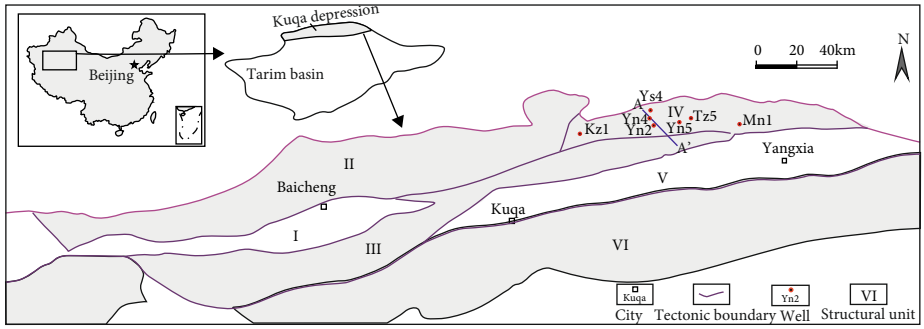

I-Baichenng sag; II-Kelasu thrust belt; III-Qiulitage thrust belt; IV-Yiqikelike thrust belt; V-Yangxia sag; VI-Luntai uplift belet

Figure 1: Regional, geological, and structural map of Dibei area in Kuqa Depression, Tarim Basin, Northwestern China (modified from [34–36]).

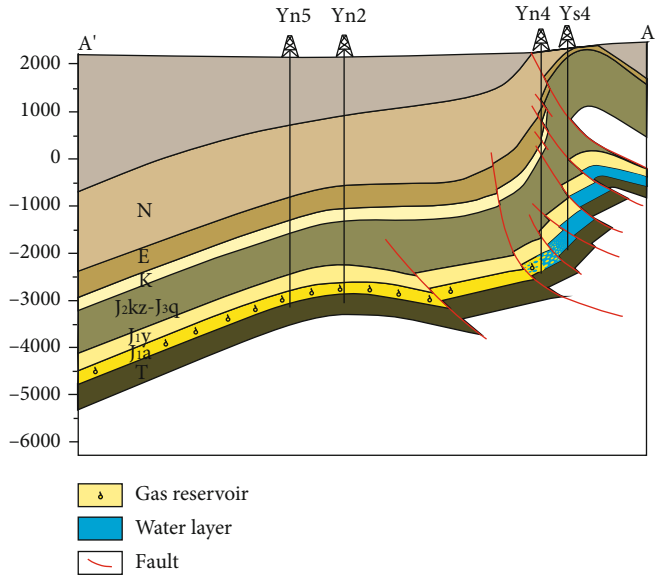

Figure 2: Structural section map of east Kuqa Depression.

Table 1: Analysis items and number of sandstone samples in the study area.

Well no.	Analysis items						
	CTS	SEM	CLSM	RCMP	HPMI	NA	PPNP and PPOP
Yn5	16	16	16	3	16	16	16
Yn2	10	10	10			10	10
Yn4	13	13	13		11	13	11
Ys4	8	8	8			8	
Kz1	2	2	2		2	2	2
Tz2	3	3	3		3	3	3
Mn1	4	4	4	1	4	4	4

data acquisition and output were carried out by the computer system. The pore structure information was obtained according to the rise and fall of mercury pressure.

3.2. HPMI. The HPMI (high-pressure mercury injection) experiment was carried out on the full automatic AutoPore IV9520 mercury injection apparatus. The pore diameter is 3 nm-1000 μm, and the volumetric accuracy of mercury injection and ejection is less than 0.1 μl; the highest injection pressure can be 414 MPa. All the samples were made into core columns and dried for 24 h before conducting this experiment.

3.3. NA. The NA (nitrogen adsorption) experiment was carried out by using the QUADRASORB SI specific surface area and porosity analyzer made by American Quanta Chrome Company. The pore diameter measuring range of the instrument is 0.35-400 nm. Before the experiment, the samples were vacuum pretreated at 150°C for 24 hours, and then, the high-purity nitrogen (with purity higher than 99.999%) was used as adsorbate to measure nitrogen adsorption capacity under different pressures at -195.8°C. Taking the relative pressure as X-axis and adsorption capacity of unit sample weight as Y-axis, nitrogen adsorption-desorption isothermal lines were drafted. According to the two BET constant formulas, the BET straight line graph with relative pressures between 0.05 and 0.35 was drawn to obtain the

specific surface area of the samples. The BJH (Barrett-Joyner-Halenda) method was applied to calculate the desorption branch of the nitrogen adsorption isothermal line to obtain the pore size distribution.

The variation law of the porosity and permeability along with the overburden pressures can be found out by the porosity and permeability analysis under net overburden pressures; therefore, the true value in formation conditions can be simulated. It is very important for tight sandstone gas reservoir with strong stress sensibility. The pressure of the reservoir in the study area is 82 MPa, and the simulated test pressure scope of the instrument is among 2.1~67.6 MPa. Affected by the instrument performance, the maximum net overburden pressure is 55 MPa. The experiment process was recorded by measuring the porosity and permeability at one point every 5 MPa. We can infer the characteristics of porosity and permeability from the variation of porosity and permeability with pressure.

4. Results

4.1. Micro-Observation Characters of Reservoir Spaces

4.1.1. Microscope. It is found that the shape and distribution of pores are obviously influenced by the microfractures. The dissolved pores are mainly developed along the microfractures (Figures 3(a) and 3(b)). The pore profiles are elongated elliptic, and their long axis directions are coincident with the extension directions of the microfractures (Figure 3(b)). Some dissolved pores can form macropores with the long axis perpendicular to the fracture due to dissolution expansion (Figure 3(a)). Another manifestation of pores affected by microfractures is "clustering development of micropores", that is, the dissolved micropores "clustered" to form a dissolution band (Figure 3(c)). Under the microscope, the micropores near the center of the band develop intensively, while the number of micropores far away from the center of the band decreases and gradually becomes isolated. However, some microfractures do not play a role in the dissolution of pores. These fractures are characterized by clean and free of impurities, parallel distribution of several fractures, large opening width of fractures (0.15~0.5 mm), and concave convex confrontation on both sides of fractures (Figure 3(d)).

The pore morphology of the Ahe Formation can be classified into three types: (1) short-axis pores: the pores are nearly round with smaller length/width ratio (Figure 3(a)); (2) long-axis pores: the pores are in apparently flat oval shape (Figure 3(b)), and the length of the long axis is 3 to 10 times of the short axis; (3) lamellar pores: the pores are in long-narrow lamellar shape (Figure 3(d)). The major pore shapes in the study area are long-axis pores and lamellar pores.

The results of cast thin section show that the primary pores of tight sandstone reservoir in Ahe Formation (J_{1a}) are not developed, and the secondary dissolution pores are scattered and isolated, with small pore radius (50 μm-150 μm) and poor connectivity between pores. The intergranular muddy dissolution micropores are well developed, followed by intergranular dissolution pores. Microfractures occupy the main pore space in some samples, and they are also one of the important types of reservoir space in the study area.

4.1.2. SEM. It can be clearly seen under SEM that the particles are filled with clay minerals of different shapes; among them, the hair and needle-like illite are the most developed (Figure 4(a)), which is symbiotically filled with the page-like kaolinite and filled between or within the particles (Figures 4(a) and 4(b)). Three types of pore-throat features can be identified: (1) pore-throats between particles and clay minerals, with a long-narrow shape (Figures 4(c) and 4(d)), and the width is between 2 μm and 5 μm. This kind of pore-throat is very common here. (2) Intercrystalline pores, mainly formed by secondary quartz overgrowth (Figure 4(e)) or developed in kaolinite (Figure 4(f), with pore diameter of about 10 μm). (3) Dissolved fractures in feldspar: the fractures are flat and discontinuous distributed along the joint surfaces of feldspar (Figures 4(g) and 4(h)). SEM observation results show that the areas displayed by dyeing agent in casting thin sections are not entirely pores; most of them are the adsorption color after being filled by clay minerals. The actual gas storage space is the intergranular pores of the clay minerals, so a more precise definition of the pore should belong to the throat. It is precisely because these clay minerals filled in the grain adsorb the dye, which is mistakenly regarded as the pore space (casting color) under the microscope, resulting in the face ratio value under the casting thin section generally larger; thus, the reservoir space of the rock is mistakenly estimated. It can be seen from Figure 4(f) that almost 90% of the pore space is filled by kaolinite and illite. Most of the reservoir spaces in Dibei gas reservoir are micropore-throats.

4.1.3. CLSM. Confocal laser scanning microscope (CLSM) can make up for the shortcomings of traditional polarizing microscope and scanning electron microscope to obtain high-definition and high-resolution images. What is more, it can clearly display and quantitatively count the micropore-throat by adding special fluorescent agent to the thin section [11, 40, 41]. Thus, CLSM has obvious advantages in the study of tight reservoir. In this study, the fractures and pores (especially the tiny throats) that are hardly observed in traditional casting thin sections are readily identified by using CLSM (Figure 5). The results show that the main reservoir spaces are microdissolution pores, and a small amount of intergranular macropores are developed. The throats are important reservoir spaces that should not be ignored and there is a close connection between pores and throats in the reservoir. The throat is distributed in network and communicated with nanopores, thus forming a tight reservoir oil and gas storage and transportation system.

4.2. Quantitative Measurements of Reservoir Space. The throat diameters of sandstone, tight sandstone, and shale are very different [13]. Therefore, different techniques are needed for further research.

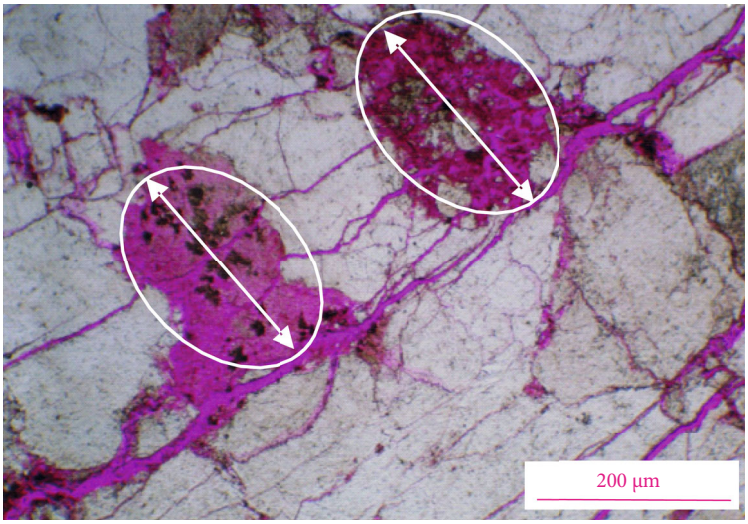

(a)

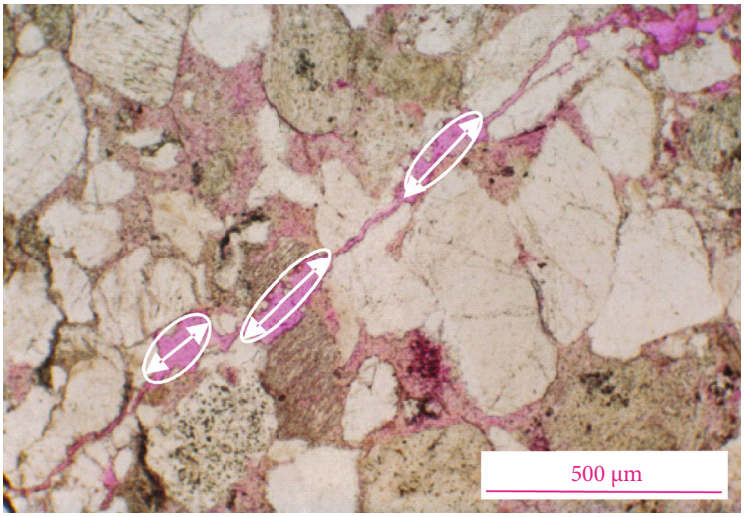

(b)

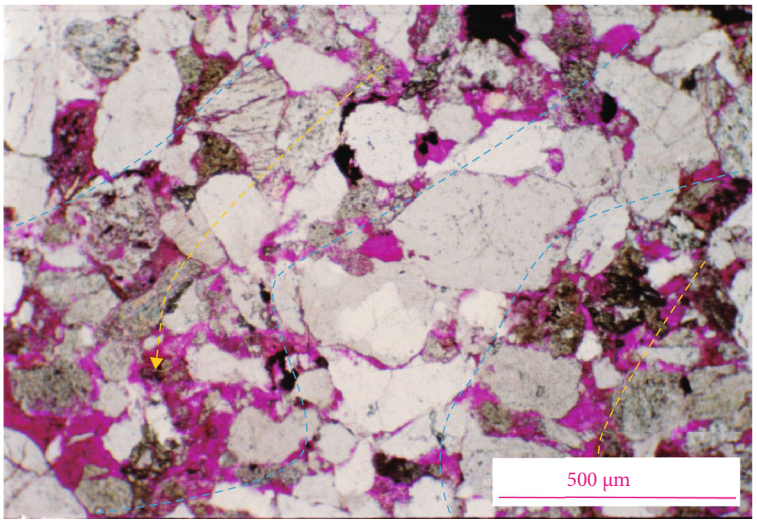

(c)

Figure 3: Continued.

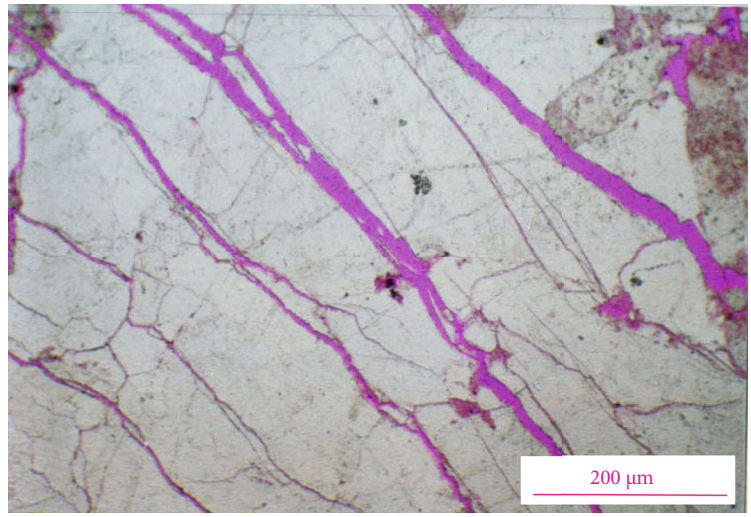

(d)

Figure 3: Thin sections of photomicrographs showing microscopic features of Dibei tight sandstone reservoirs in Ahe Formation. (a) Well Yn5, J_1a, brachy pores: the pores are intersected by fractures and are nearly in rounded shape. (b) Well Yn2, J_1a: the pores are developed in flat and long-axis shape. (c) Well Yn4, J_1a: the secondary dissolved micropores are developed in clustering and banding form. (d) Well Yn5, J_1a: the microfissures are nearly parallel with bigger openness, without impurity between fissures.

4.2.1. Rate-Controlled Mercury Penetration. The RCMP has an obvious advantage in evaluating pores and throats, especially for tight sandstone reservoir, which can effectively reflect the number, size, and distribution characteristics of pores and throats [42, 43]. Compared with conventional mercury penetration technique, the RCMP can inject mercury into rock pores at very low and constant rate (generally 0.00005 ml/min). By detecting the pressure fluctuation during the mercury penetration, the RCMP can separate pores and throats in rocks; thus, the detection results can provide the capillary pressure curves of pores and throats and obtain the rock microstructure characteristic parameters such as pore radius distribution, throat radius distribution, and radius ratio of pore-throat distribution.

The throat saturation values of the tight sandstone samples (except for sample Yn5-3) in the Ahe Formation are obviously higher than the pore saturation values (Table 2), which is quite different from the analysis results of conventional sandstone reservoirs. The saturation values of pores of conventional sandstone reservoirs are higher than those of throats, which may be caused by the development of microfractures. Figure 6 shows the distribution feature of the throats and pores in sample Yn5-2 with RCMP. It can be seen that the main peak value of the throat radius is 1 μm, and the main peak value of the pore radius is among 125~150 μm.

4.2.2. High-Pressure Mercury Injection. In conventional mercury penetration analysis, the mercury injection pressure is generally less than 50 MPa, and the minimum throat radius that mercury can enter is about 0.01 μm. However, the throat radius value in tight sandstones is widely distributed, with a minimum of 10 nm [13]. Hence, the conventional mercury penetration data cannot truly reflect the distribution feature of throats in reservoirs. The maximum injection pressure of HPMI can reach as high as 400 MPa; therefore, it can be used to approximately reflect the whole distribution scope of the throats.

In view of the fact that there are many fractures in the sandstone samples, the high pressure can easily damage the samples during the injection process. Therefore, 200 MPa of the mercury injection pressure was selected in this study. The minimum throat radius under 200 MPa pressure is 3.7 nm, which is basically close to the size of the oil and gas molecules. The data of 27 samples shows that the average mercury injection saturation is 67.2%, and the maximum mercury injection saturation is 87% (Figure 7). Though they are apparently higher than that reflected by conventional mercury penetration data, it is still unable to achieve 100% mercury injection saturation. The main reason is that there are invalid pores in the sample, and the throats which connected by these pores are much smaller, or these pores are isolated from the throats and fail to communicate with the pore-throat network. However, these invalid pores still occupy part of the pore volume, so that the pores cannot be fully filled by mercury penetration. Such deficiency can be overcome by the combination of HPMI and nitrogen adsorption techniques to comprehensively obtain the unavailable pore space volumes in samples.

4.2.3. Nitrogen Adsorption Isotherm Analysis. The NA test method can make up for the shortage of other analysis and test on the observation of micropore and can focus on the distribution characteristics of throat radius below 100 nm; thus, it has a good effect on identifying the micropore and throat features in tight reservoirs [44, 45].

The results of nitrogen adsorption and desorption isotherms (Figure 8) show that the distribution status and shape of the pores and throats can be qualitatively evaluated by the shape of the adsorption isotherm. According to the classification of International Union of Pure and Applied

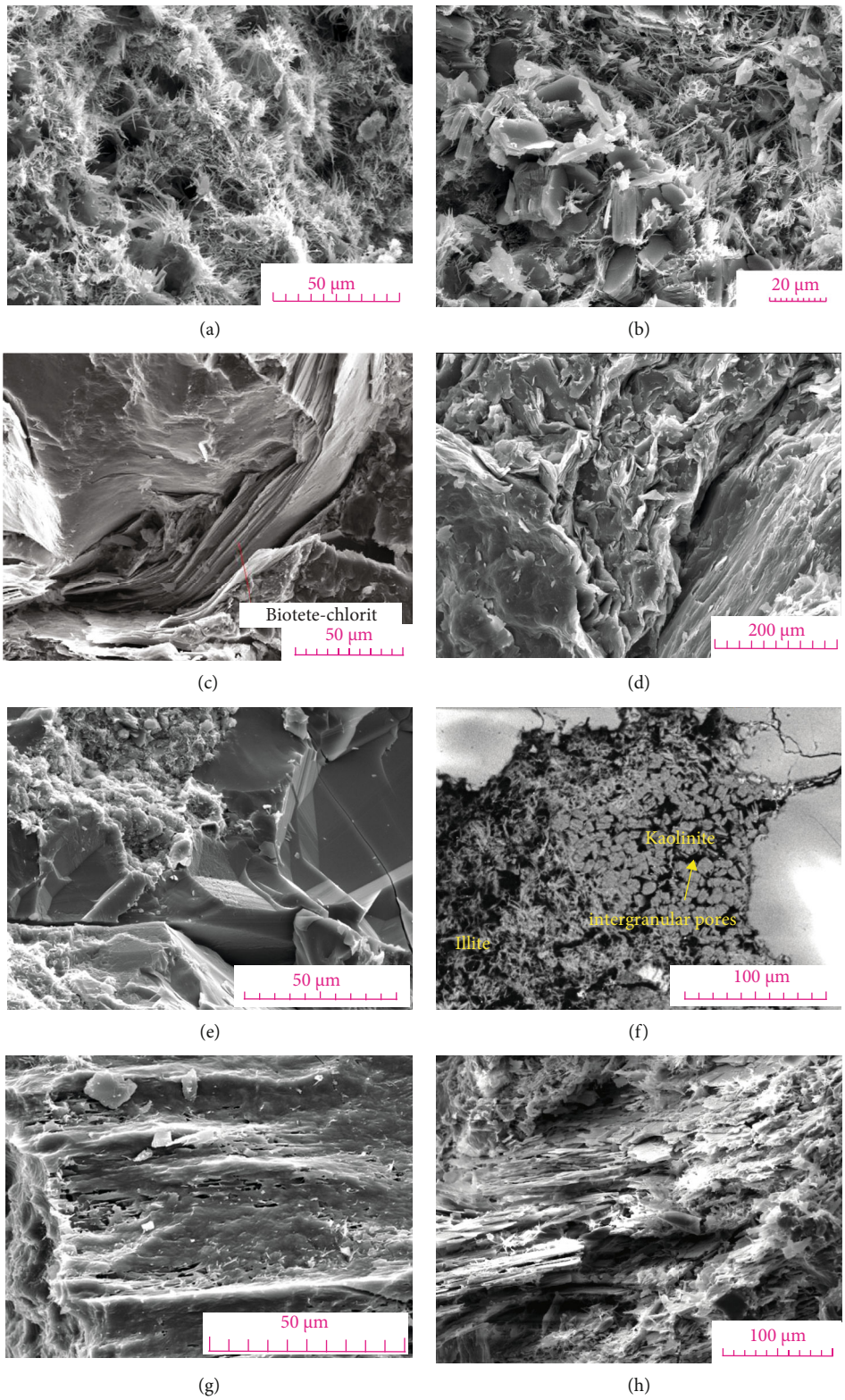

Figure 4: Scanning electron microscope photomicrographs showing pore space and morphology of minerals filled in space in the Ahe Formation of Dibei area. (a) Yn2, J_1y, 4538.31 m: intergranular fibrous illite and smectite mixed layers. (b) Yn5, J_1y, 4562.8 m: kaolinite in book-like form and illite in hair-like form. (c) Yn5, J_1y, 4562.8 m: pores and fissures between lamella biotite and chlorite minerals. (d) Yn5, J_1y, 4562.8 m: long-narrow fissures between grains. (e) Yn, J_1a, 4851.8 m: intercrystalline pores between secondary quartz crystals. (f) Ys4, J1a, 3981.6 m: kaolinite and illite filling between grains in thin sections under SEM. (g) Yn5, J_1a, 5007.1 m: the dissolved micropores in feldspar are developed along joint seams. (h) Yn5, J_1a, 4775.23 m: flat fissures are formed by corrosion along joint seams in feldspar.

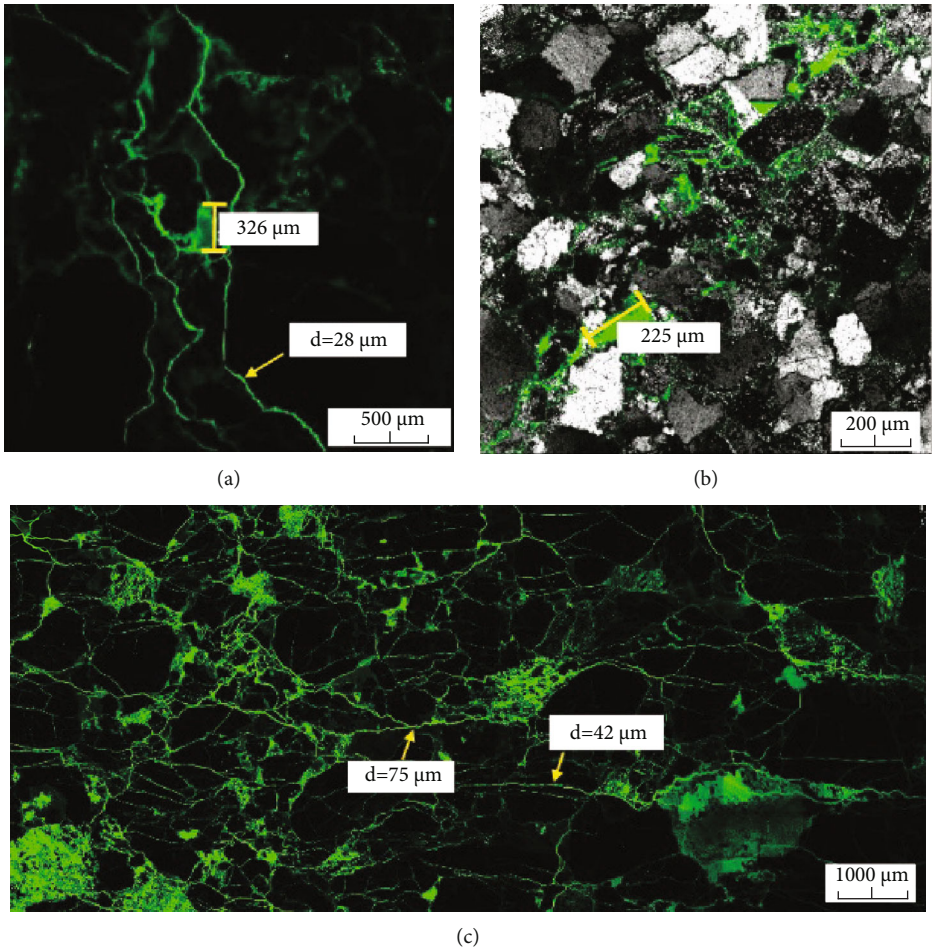

Figure 5: Scanning laser confocal microscope photomicrographs showing slot pore characteristics in the Ahe Formation of Dibei area. (a) Well Yn2: clear structural fractures. (b) Well Yn2, J_1a: corroded bands with clustering tiny corrosion pores. Tiny pores are clear. (c) Well Yn5, J_1a: a thin section image of scanning laser confocal microscope, showing connected throats and corroded pores in network style.

Table 2: Result of rate-controlled mercury penetration in the study area.

No.	Yn5-1	Yn5-2	Yn5-3	mn1-1
Gasometry porosity (%)	9.30	6.96	8.18	19.65
Gasometry permeability (10^{-3} μm^2)	1.06	0.293	11.030	14.360
Apparent rock density (g/cm^3)	2.42	2.49	2.44	2.12
Bulk volume of rock sample VB (cm^3)	1.77	3.41	4.48	1.88
Pore volume of rock sample VP (cm^3)	0.16	0.24	0.37	0.37
Penetrated mercury saturation in throat (%)	26.70	25.44	28.29	41.02
Penetrated mercury saturation in pore (%)	10.08	10.89	29.48	23.18
Total penetrated mercury saturation (%)	36.78	36.33	57.77	64.20

Chemistry (IUPAC), the form of the adsorption isotherm of the Dibei reservoirs is type IV. The adsorption isotherm is different from the desorption isotherm, and the hysteresis loop can be seen. A platform can be observed in the area with high P/P_0 value (greater than 0.4), and it ends up with the isotherm upward. This type of isotherm indicates that the samples in this area are chiefly medium pores (the diameters of the medium pores are between 2 and 50 nm, according to the classification of IUPAC). The pores in this order cannot be observed in other analytical methods.

4.2.4. Routine and Stress-Dependent Core Analysis. It is very important to evaluate the influence of pore-throat morphology on tight gas reservoir quality under formation pressure, because low-permeability reservoirs are very sensitive to the confining pressure [23, 46]. The permeability values measured under normal pressures cannot truly reflect the reservoir seepage capacity under formation pressure [16]. Related statistics show that the permeability under overburden pressures is only 1/10 of that under normal pressure. The sandstone samples of the gas reservoir in Dibei area also show

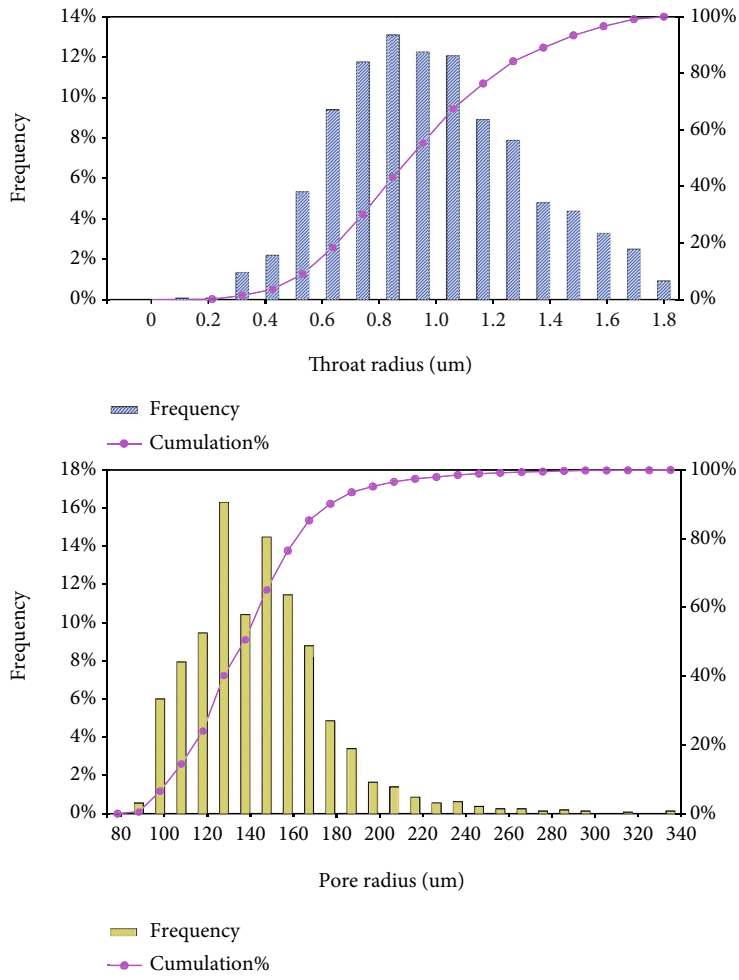

Figure 6: Distribution feature of throats and pores in reservoirs of Yn5-2 samples.

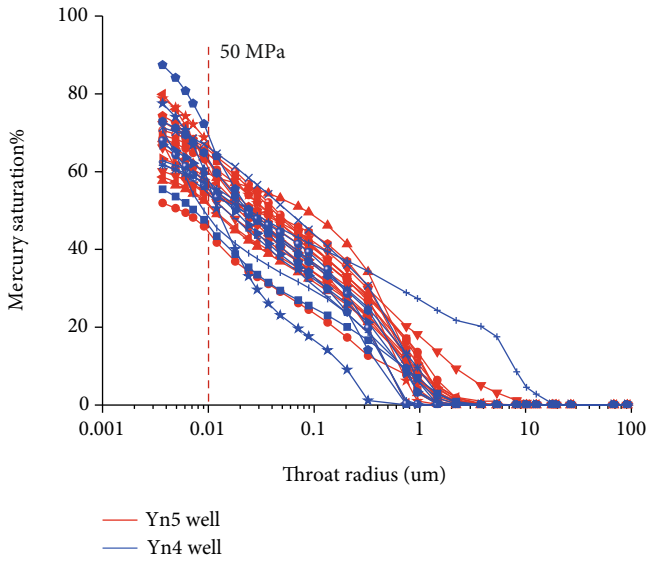

Figure 7: HPMI curve feature of tight sandstone reservoirs in Dibei area.

that the permeability value under overburden pressure is much smaller than that under normal pressures. However, there is a great difference in the variation trend of permeability of different samples under the overburden pressure.

Figure 9 shows that the permeability values of the samples in type II and III under overburden pressure (50 MPa) are almost less than 0.1 mD, which is 1-2 orders of magnitude lower than that under normal pressures, while the permeability values of the loose samples in type I did not change. On the contrary, the porosity value of the loose samples in type I decreases obviously under overburden pressure, while that of the samples in type II and III has no obvious change. Dibei tight gas reservoir is dominated by type II reservoir, followed by type III reservoir.

4.3. Pore-Throat Morphology of Tight Sandstone Reservoirs. Primary pores in the tight sandstone of the Ahe Formation are not well developed under the microscope. The dissolved pores are generally distributed in isolation, with the pore radius of 50 to 150 μm, and the connectivity of intercrystalline pores is poor. The main dissolution pores are the intergranular dissolution pores, followed by the intragranular dissolution pores, which are developed in feldspar grains and volcanic debris grains. Microfractures occupy the main

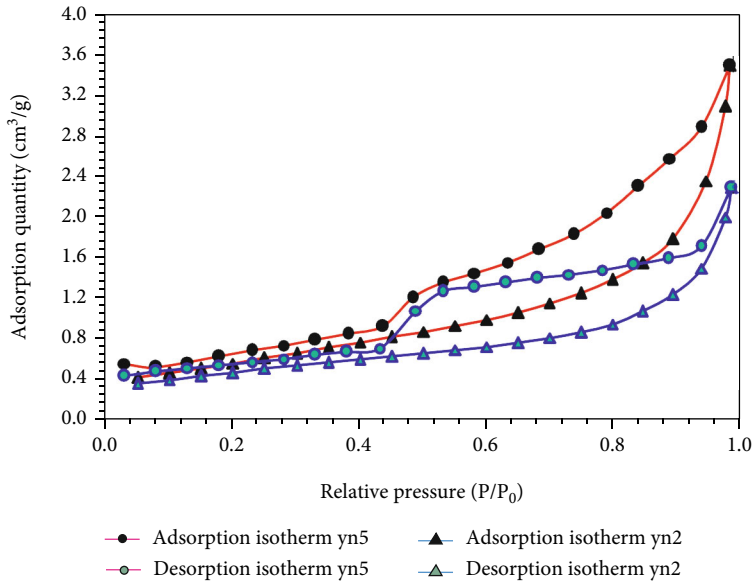

Figure 8: Low-temperature nitrogen adsorption and desorption isotherm for tight sandstone in the study area.

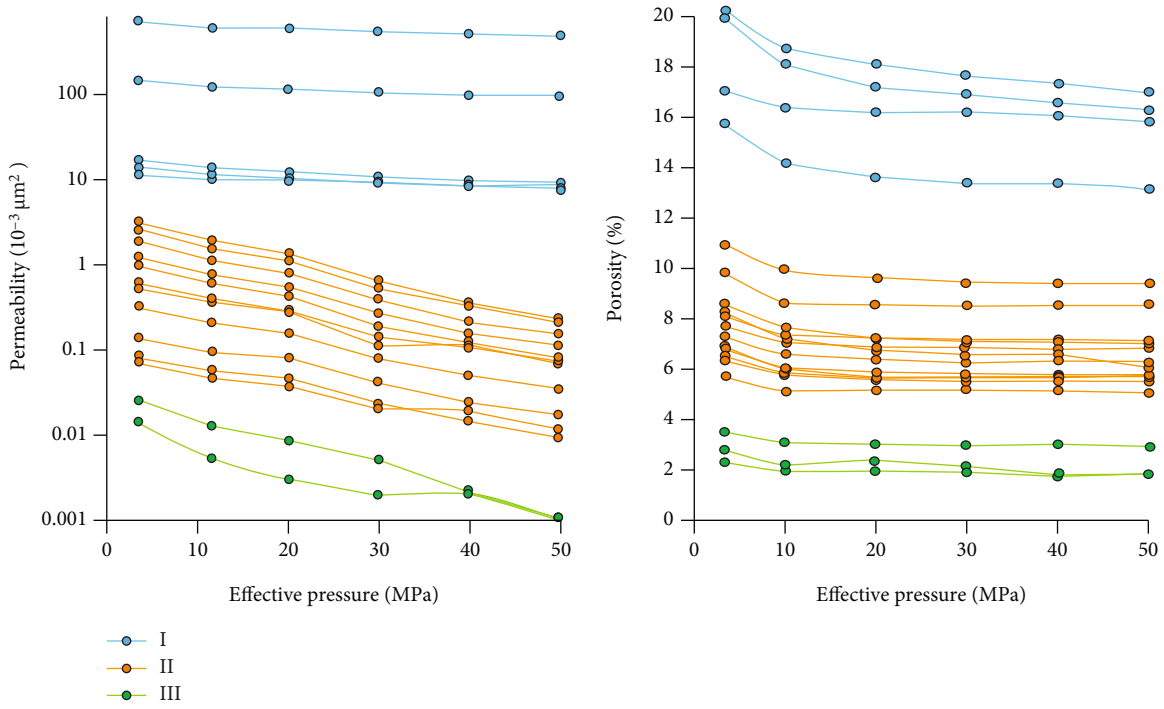

Figure 9: Correlation between porosity and permeability under overburden pressure of tight sandstone samples in the Dibei area.

pore space of some samples and are also one of the main reservoir space types in this area.

The hysteresis loop of nitrogen adsorption test (Figure 8) can reflect the features of sample pore-throats. It can be divided into four types, and different types reflect different morphological features of the pore-throat. According to the hysteresis loop (desorption curve), there are two major types of pore morphology in the samples. (1) inkbottle-shaped pores with small caliber and wide body, and the big pore-throat is unfavorable for gas seepage and (2) pores in plate and flat shape; this type of sample is generally composed of flake particles, such as clay or clustered micropores. This conclusion is consistent with the morphological features previously observed intuitively, indicating that the tight reservoirs in the study area are mainly composed of micropore in intergranular clay minerals, followed by the long-narrow and flat throats.

4.4. Pore-Throat Sizes and Distribution in Tight Sandstones. Rate-controlled mercury penetration (RCMP) and high-

pressure mercury injection (HPMI) are effective methods for analyzing pore-throat radius from different perspectives. It can be concluded from the result of RCMP that the throat radius in tight sandstones is mainly distributed in the range of 0.4-2 μm (the main peak is at around 1 μm), and the pore radius is distributed in a wider scope of 75-350 μm (the main peak is among125-150 μm) (Figure 6). The peak value of the pore-throat ratio ranged from 40 to 150 μm. They are generally represented as the shape of small caliber with wide body.

The average pore-throat radius distribution reflected by the HPMI testing (Figure 10) shows that the peak of the pore-throat radius is around 0.324 μm, and most pore-throats radii are smaller than 2 μm. To carry out HPMI and NA tests for the same sample, taking the data of two methods in the same coordinate system for mapping, it can well reflect the widest range of the pore-throat radius distribution in the tight sandstone samples. Figure 11 shows the average pore-throat radius distribution graph by matching the data of HPMI and NA of 27 samples. The NA testing results show that abundant micropores with radius smaller than 50 nm are still developed and their total pore volume accounts for more than 15% of the total pore volume.

5. Discussion

5.1. Throats Are the Major Storage Spaces for Tight Sandstone Gas Reservoir. RCMP data of four samples shows that the throat radius of the reservoirs in Dibei area ranges from 1 μm to 4 μm (Figure 11(a)), and the peak ratios of pore-throat radius range from 40 to 150 (Figure 11(b)). The average mercury injection saturation of gas reservoirs is 48.77%, in which the average mercury injection saturations of pores and throats are 18.4% and 30.37%, respectively. Thus, throats contribute more than 60% of the total gas spaces. The throats not only play the role of connecting the pores and throats but also are the major reservoir spaces in tight gas reservoirs. It is obviously different from the cognition that pores are the major reservoir spaces in conventional reservoirs.

According to the pore radius calculation formula (BJH), the pore radius distribution scope and pore volumes of the samples in nitrogen adsorption test are obtained (Figure 11). The volumes of the pores with 2-50 nm account for more than 14.3% of the total pore volume. Under the HPMI condition, 40% of the pore-throat volume cannot be measured. Even if it is assumed that the adsorption test can identify the total connected throat volume, nearly 30% of the pores still cannot be identified by existing technology, which is considered as the isolated and invalid pores in samples. According to the NA test results of 56 samples, the throat volumes below 50 nm account for about 45% of the total porosity, micropores (<2 nm), and mesopores (2-50 nm), and ineffective pores occupy 64% of the pore space [47].

5.2. The Effect of Throat Morphology on Reservoir Seepage Capacity. Pore-throat morphology is an important parameter for reservoir evaluation. Some researchers have attempted to study the characteristics of complex pore structure by fractal geometry theory [48, 49]. In fact, pore-throat morphology is random and disordered, and accurately, descriptions remain uncertain. In this study, pore-throat morphology can be distinguished by the curves of the adsorption and desorption in nitrogen adsorption test, which is a comprehensive reflection of all pore-throat morphology (Figure 8). The radius ratio of the connecting pore-throat and the length/width ratio of pores (or throats) are used to simply characterize the pore-throat morphology (Figure 11(b)). Figure 11(a) shows the percentage of the throats with different radius in the samples. It does not display the shape of the pore-throat, but only the size of the throat. The wider the curve is, the larger the throat exists in the sample. Figure 11(b) shows the distribution range and frequency of the ratio of pore radius to throat radius, which represents the shape of the pore-throat. The larger the ratio is, the more asymmetric the pore-throat is, such as the inkbottle-shaped pore-throat (with small caliber and wide body). The smaller the ratio is, the more regular the shape of pore-throat is, such as oval and round shape. When the ratio is about 100, the pore-throat is flat and slender strip.

The peak of the pore-throat ratio in sample mn1-1 with permeability value of 14.36 mD is located in the horizontal coordinates of 40. With the decrease of permeability, the pore-throat ratio corresponding to the peak increases gradually. It can be seen that the primary peak is 150 when the permeability is 0.29 mD (sample Yn5-2). Therefore, the primary peak position of the pore-throat ratios is closely related to the permeability value, indicating that the permeability is not only affected by pore-throat size, but also by pore-throat morphology, although it can be seen from Figure 11(a) that the permeability value has a certain correlation with the throat size of the reservoir; for example, the larger the permeability value of the sample, the larger the proportion of the large throat. The morphology of pore-throat reflected by the ratio of pore-throat is the indicator of reservoir seepage ability. The effect of the throat on the seepage capacity is only shown as the slippage effect of gas when the throat radius is small, resulting in smaller permeability value [50]. However, it is the ratio of pore-throat, that is, the shape of pore-throat, that really reflects the seepage capacity of reservoir.

By comparing the pore-throat shapes of type I, II, and III samples, it is considered that the main reason for the differences of porosity and permeability under overburden pressure is the closure effect of the long-narrow and flat throats, followed by the blockage effect of clay minerals on the throats. The porosity of the samples in type I under normal pressure is bigger than 15%, mainly developing big-radius pores (their diameters are generally among 0.2-0.5 mm), with smaller length/width ratios (about 1). The relationship between grains is point contact or line contact, and the grains in some samples are suspended. Due to the development of pore space, the change of grain framework under overburden pressure results in the decrease of pore space and porosity. However, there is still plenty of seepage space among the grains, and the decrease of seepage capacity of fluid is much limited. For the type II samples of tight

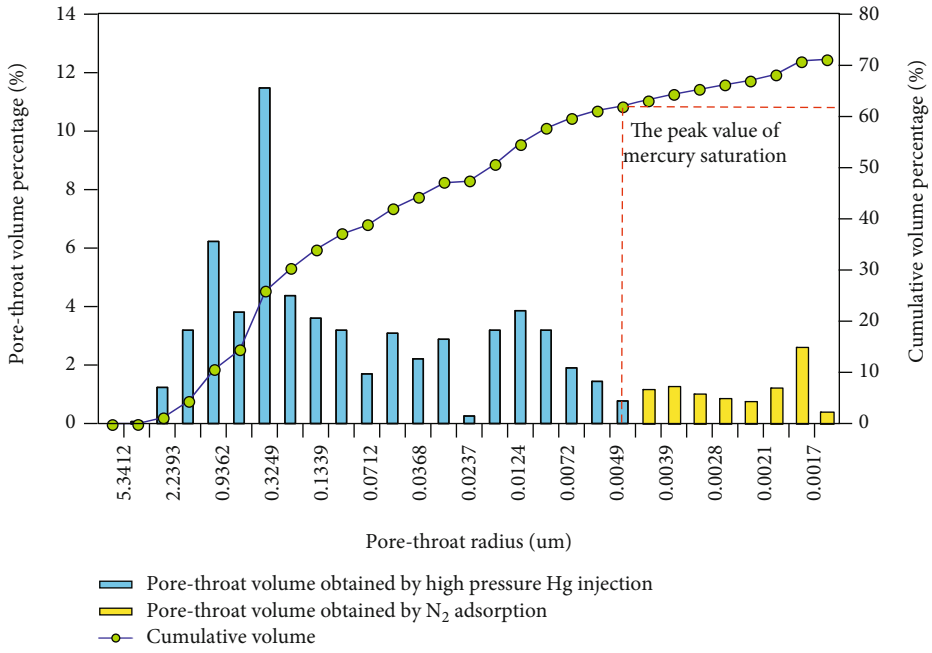

Figure 10: Pore-throat radius distribution features in high-pressure mercury penetration and nitrogen adsorption.

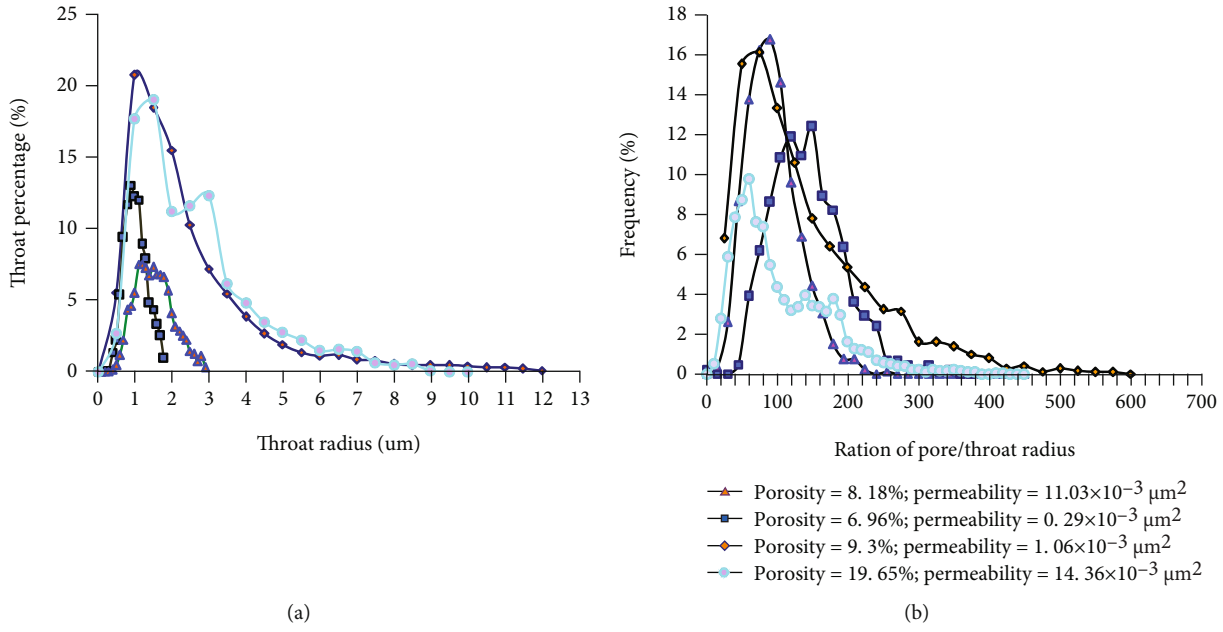

(a) (b)

Figure 11: Distribution of throat radius and ratio of pore-throat radius for tight sandstones of different porosity-permeability properties.

sandstone, the decrease of pore spaces in reservoirs under overburden pressure is mainly reflected in the closure effect of the long-narrow and flat micropore-throats or compression into narrower pore-throat. For the total pore-throat space, the decreased volume may be smaller, but for the seepage capacity of pore-throats, the decrease of the space can directly result in the closure of the throat and the increase of the fluid slippage effect, which seriously affects the fluid seepage capacity. Therefore, the long-narrow space with large pore-throat ratios in reservoirs has apparent influence on reservoir quality.

In tight sandstones, the reservoir quality is relatively sensitive to clay minerals and the existence of clay minerals can seriously block the microthroats. For the reservoir of this long-narrow pore-throat type in this area, the clay minerals aggravate the plugging of pore-throat and seriously hinder the flow of fluid. There are lots of muddy matrices in type III samples. The matrix is mainly primary clay minerals.

The pseudo matrix phenomenon occurred during the process of compaction can seriously reduce the pore spaces. Improper modification measures in the drilling may aggravate the blockage of the throats. Due to the strong acid sensitivity of the reservoir in this area, the later acid fracturing process is easy to cause reservoir pollution, thus missing the discovery of the gas layers. At present, the nitrogen drilling technology can effectively protect the reservoirs in the Dibei area, so that the discovery rate and drilling success rate of gas layers during later period are significantly improved.

5.3. Determination of Cutoff Value of Throat Radius. Throat radius is the key factor for controlling gas seepage capacity in reservoirs. The fluids in different throat radius intervals have great differences of flow modes and seepage capacity. The results of HPMI experiments show that the pore spaces with the throat radius > 0.3 μm in tight sandstone samples contribute more than 98% of the fluid permeability. If 98% of the fluid flow capacity is taken as the free flow space of reservoir throats [51], then 0.3 μm throat radius is the minimum value of free fluid pore space. When the throat radius in reservoirs is greater than 0.3 μm, the fluids in the space can be naturally produced without external force, and this part of gas corresponds to the natural gas production during the exploitation of tight sandstone reservoirs.

As the space with radius larger than 0.3 μm is in a small proportion, the porosity and permeability of the tight gas reservoirs are low, and the gas productivity under natural condition is very limited. Therefore, it is necessary to stimulate the reservoirs, such as fracturing, to improve the productivity of single well. In the process of stimulation, the reservoir throats are actually widened, so that the gas bounded in the smaller throat in the early stage can be released to form productivity. Further detailed studies are still needed to determine whether the throats with radius smaller than 0.3 μm can be entirely stimulated into actual production capacity. In this study, the minimum movable fluid pore radius (i.e., the lower limit of throat radius for reservoir stimulation) in reservoirs can be determined by a nuclear magnetic centrifuged laboratory experiment.

Centrifuged experiment for the brine-saturated samples can be used to calibrate the T2 cutoff value of the movable fluid in tight sandstones [52]. In this paper, the magnetic resonance experiments under various centrifugal conditions were carried out, and it found that with a gradual increase of centrifugal force, the movable water in water-saturated samples was gradually expelled. When the centrifugal force reached 2.75 MPa, there is almost no difference (or very small difference) between the T_2 spectrogram curve and the spectrogram curve at 2.42 MPa. Thus, it can be concluded that 2.75 MPa is the limited value of the movable water that can be expelled from tight sandstones by centrifugal force. This means that the throat radius corresponding to 2.75 MPa is the minimum throat radius for the movable fluid in samples (Figure 12). As there is capillary force balance between porous medium and water when the water is subjected to centrifugal force, it is necessary to convert the interaction between water and capillary into that between

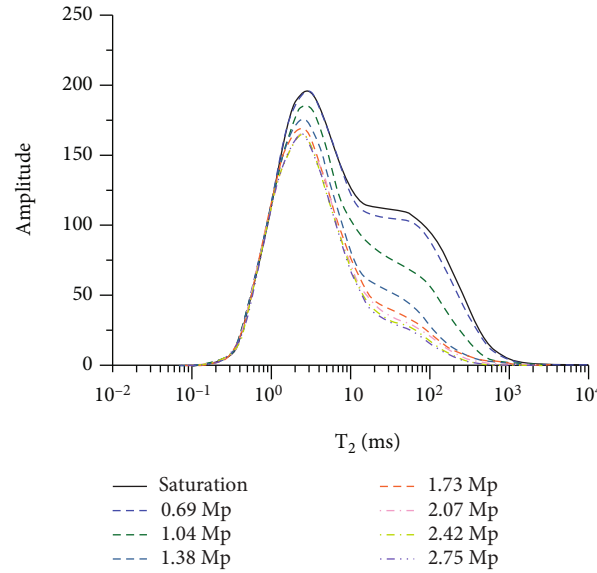

Figure 12: T_2 spectrogram curve in various pressures for tight sandstones in study area.

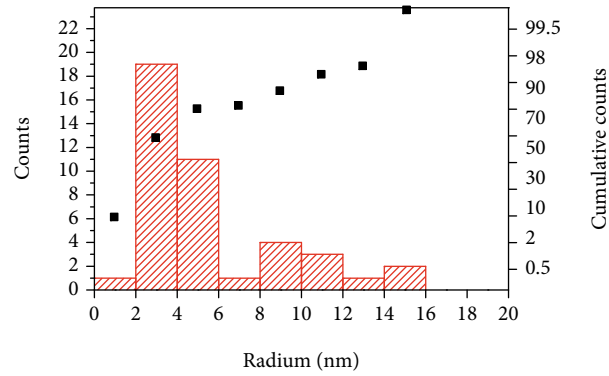

Figure 13: Distribution graph of immobile water film thickness in cores of tight sandstone in Dibei area.

gas and capillary. The capillary force formula in porous medium is as follows:

$$P_c = \frac{2_{\rho \cos \theta}}{r}, \quad (1)$$

where P_c is the capillary force in porous medium (MPa). ρ is the interfacial tension between gas and water, which is 72 N/m under normal condition. θ is the wetting angle, being 0° for gas-water centrifuge. r is the pore-throat radius (mm).

According to Equation (1), the corresponding throat radius is 0.052 μm under the centrifugal condition of 2.75 MPa. Thus, it can be considered that the pore space with throat radius among 0.3-0.052 μm in tight sandstone reservoirs can be converted to be movable fluid after reconstruction, and 0.052 μm is the cutoff value of working movable fluid.

Theoretically, as long as the throat radius in reservoirs is larger than that of the gas, it can be used as the gas storage space. In fact, due to the existence of bound water in the

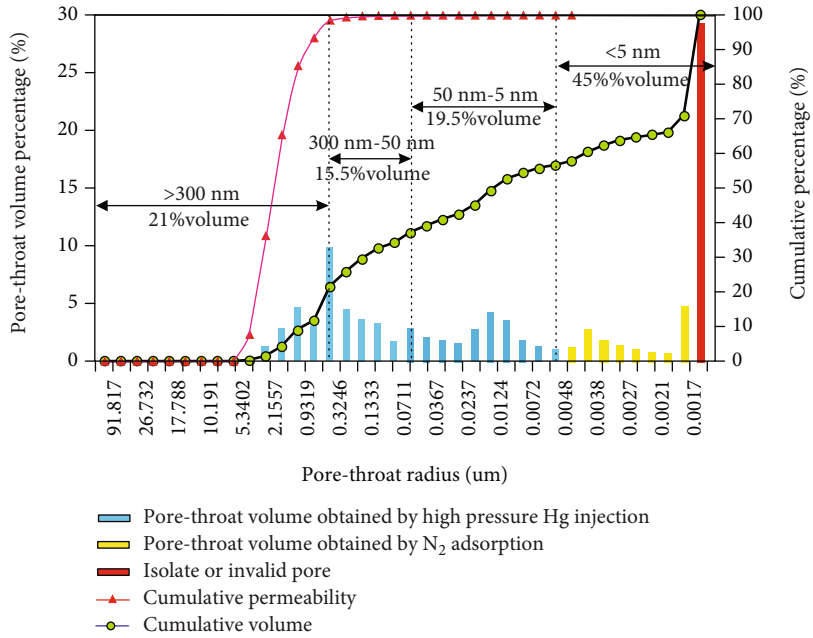

Figure 14: Distribution of pore-throat radius, cut off values, and their percentages in total pore spaces in tight sandstone reservoirs of Ahe Formation in Dibei area.

Table 3: Calculation parameters and results of tight sandstone gas reserves in Dibei area.

Gas-bearing area (km^2)	Net thickness (m)	Net porosity (%)	Gas saturation (%)	Volume factor	Geologic gas reserves ($10^8\ m^3$)	Recoverable gas reserves ($10^8\ m^3$)
35.2	102.1	6.7	63	0.00267	568.2	284.1

reservoir, the water film of the irreducible water can block the pore-throats and prevent the invasion of the gas.

When the pore-throats are blocked by the bound water, the throat radius which is equal to the thickness of the bound water film on the two walls is the low limit of the throat radius for natural gas injection, so the thickness of the bound water film can be used as the low limit of the pore-throat radius for natural gas injection [53]. The formula for the thickness of bound water film is as follows:

$$d_i = 7142\Phi * \frac{S_{wi}}{A_i * \rho}, \quad (2)$$

where d_i is the bound water film thickness (0.1 nm). φ is the core porosity (%). S_{wi} is the bound water saturation (%). A is the specific surface area of core (m^2/g). ρ is the core density (g/cm^3).

Figure 13 is the distribution graph of bound water film thickness calculated by Equation (2) of 42 cores in this area. The major bound water film thickness in pore-throats is about 5 nm. Thus, 5 nm can act as the lower limit for gas charging in tight reservoirs.

Figure 14 shows the distribution range of throat radius and the percentage of pore volume occupied by different throat radius in tight sandstone reservoirs. The free fluid pore volume with throat radius that exceeds 300 nm accounts for 21% of total pore volume. The storage space with throat radius among 300-50 nm that can be reconstructed to obtain movable fluid accounts for 15% of total pore space. The reservoir space of irreducible fluid with low-limit throat radius among 50-5 nm for gas charging accounts for 19% of total pore space. The isolated and invalid pore space accounts for 45%.

5.4. Calculation of Geological Reserves and Recoverable Reserves. The calculation of tight gas reserves is based on the following formula:

$$G_c = 0.01 \times A_g \times h \times \Phi \times S_{gi} \times \frac{1}{B_{gi}}, \quad (3)$$

where G_c is the total geological reserves of condensate gas ($10^8\ m^3$). A_g is the gas-bearing area (km^2). h is the average effective thickness (m). Φ is the average porosity (%). S_{gi} is the initial gas saturation (%). B_{gi} is the original gas volume factor.

The calculation parameters of reserves in the study area are shown in Table 3. According to Equation (3), the geological reserves of natural gas in this area can be calculated to be $568.2 \times 10^8\ m^3$. The recoverable reserves are $284.1 \times 10^8\ m^3$ by the classification method and 50% of other gas parameters of the basin.

Table 4 shows the geological reserves and recoverable reserves of natural gas calculated by using the gas-bearing

Table 4: Calculation parameters and results of tight sandstone gas reserves by throat method.

Area	Gas-bearing area (km^2)	Net thickness (m)	Net porosity (%)	Net pore space (%)	Movable fluid pore space (without stimulation) (%)	Movable fluid pore space (after stimulation) (%)	Volume factor	Geologic gas reserves ($10^8\ m^3$)	Natural recoverable gas reserves ($10^8\ m^3$)	Recoverable gas reserves after stimulation ($10^8\ m^3$)
Dibei	35.2	102.1	6.7	55	21	36.5	0.00267	496.01	189.39	329.17

interval of throat in Figure 14. Compared with Table 2, the geological reserves of natural gas decreased by 12.7% to 496.01×10^8 m^3, but the recoverable reserves increased by 15.87% to 329.17×10^8 m^3, of which the natural gas produced without transformation was 189.39×10^8 m^3, and the production increased by 139.79×10^8 m^3 after transformation. Therefore, for tight sandstone gas reservoir, fracturing is very necessary.

6. Conclusions

Various methods are used to characterize the pore-throat of the tight sandstones in the Kuqa Depression, and the relationship between reserves and productivity with throat is discussed. The main conclusions drawn from this thesis are as follows:

(1) The sandstone gas reservoirs in the Dibei area are tight, with high matrix content and abundant clay minerals. The major reservoir spaces are long-narrow and flat pore-throats and the clay mineral intergranular micropores

(2) The throat radius in reservoirs is mainly distributed between 1 and 4 μm, and the throats account for nearly 2/3 of spaces of the tight sandstones. The shape of the pore-throat directly affects the production capacity of the reservoir

(3) The pores with throat radius greater than 300 nm have free fluid, and they contribute more than 98% of the reservoir permeability. The pore spaces with throat radius between 300 nm and 52 nm can expel fluids by stimulation. The pore-throats with radius < 52 nm cannot release the irreducible hydrocarbon fluids even if they have been charged with hydrocarbons, and they are inefficient pore-throats. Such pore-throats account for 65% of the tight sandstone reservoirs in the Dibei area

(4) Under the formation pressure, the tight sandstone reservoir with long-flat pore-throat is easy to have the closure of the throat and the compression circulation space, which makes the seepage capacity decrease sharply. In addition, the clay minerals in pore-throats can lead to more serious blocking effect, which hinders the fluid seepage

(5) According to the pore-throat distribution characteristics of tight sandstone reservoir, the calculation of tight gas geological reserves and recoverable reserves is carried out. There are some differences between this calculation result and the conventional calculation result, which is reflected in the reduction of geological reserves by 12.7% and the increase of recoverable reserves by 15.87%

Data Availability

Analysis of diagenetic system and pore evolution of clastic reservoir (ID: 2021DJ0402) is available upon reasonable request from the corresponding author.

Conflicts of Interest

The authors declare that they have no conflicts of interest.

References

[1] D. J. Hartmann and E. A. Beaumont, "Predicting reservoir system quality and performance," in *Exploring for Oil and Gas Traps: AAPG Treatise of Petroleum Geology: Handbook of Petroleum Geology*, E. A. Beaumont and N. H. Foster, Eds., pp. 9–154, AAPG Special, 1999.

[2] W. Yang, Z. Y. Xie, and H. Jin, "Reservoir evaluation and pooling mechanism of the Xujiahe Formation in the Sichuan Basin," *Natural Gas Industry*, vol. 30, no. 12, pp. 10–15, 2010.

[3] Y. F. Yang, K. Wang, Q. F. Lv et al., "Flow simulation considering adsorption boundary layer based on digital rock and finite element method," *Petroleum Science*, vol. 18, no. 1, pp. 183–194, 2021.

[4] L. Zheng, Z. J. Jin, and S. N. Zhang, "Features and evaluation of the Paleozoic tight sandstone reservoirs of the Rub Al Khali Basin in the Middle East," *Oil and Gas Geology*, vol. 34, pp. 475–482, 2013.

[5] C. Cheng, K. F. Lu, and X. K. He, "Based on the R35 of mercury injection data to quantitative classification, evaluation and reservoir characteristics–a case study of E15 layer in X field," *Journal of Oil and Gas Technology*, vol. 36, pp. 16–20, 2014.

[6] M. Y. Feng, T. Liu, T. Lin, X. H. Liu, N. X. Li, and A. H. Xi, "Fracture fillings and implication of fluid activities in volcanic rocks: Dixi Area in Kelameili Gas Field, Junggar Basin, Northwestern China," *Minerals*, vol. 9, no. 3, p. 154, 2019.

[7] J. J. Sun, H. K. Guo, and W. Liu, "Characteristics of micro pore-throat in low permeability volcanic gas reservoir," *Fault-Block Oil & Gas Field*, vol. 17, pp. 548–552, 2010.

[8] D. S. Guang, *China's Unconventional Oil and Gas Geology*, Petroleum Industry Press, Beijing, 1995.

[9] J. J. Li, Y. Liu, Y. J. Gao, B. Y. Cheng, and H. Q. Jiang, "Pore-scale study of the pressure-sensitive effect of sandstone and its influence on multiphase flows," *Petroleum Science*, vol. 16, no. 2, pp. 382–395, 2019.

[10] Z. Li, Y. Duan, Q. Fang, and M. Wei, "A study of relative permeability for transient two-phase flow in a low permeability fractal porous medium," *Advances in Geo-Energy Research*, vol. 2, no. 4, pp. 369–379, 2018.

[11] T. Lin, S. W. Yi, M. L. Ye, Q. G. Ran, H. X. Wei, and W. H. Liu, "Characteristic of tight sandstone gas reservoir and the enrichment regularity in eastern Kuqa Depression," *Geological Science and Technology Information*, vol. 33, pp. 116–122, 2014.

[12] R. M. Slatt and N. R. O'Brien, "Pore types in the Barnett and Woodford gas shales: contribution to understanding gas storage and migration pathways in fine-grained rocks," *AAPG Bulletin*, vol. 95, no. 12, pp. 2017–2030, 2011.

[13] P. H. Nelson, "Pore-throat sizes in sandstones, tight sandstones, and shales," *AAPG Bulletin*, vol. 93, pp. 329–340, 2009.

[14] E. D. Pittman, "Relationship of porosity and permeability to various parameters derived from mercury injection-capillary pressure curves for sandstone1," *AAPG Bulletin*, vol. 76, pp. 191–198, 1992.

[15] R. Aguilera, "Incorporating capillary pressure, pore aperture radius, height above free water table, and Winland r_{35} values on picket plots," *AAPG Bulletin*, vol. 86, pp. 605–624, 2002.

[16] M. Y. Hu, S. X. Li, and G. Q. Wei, "Reservoir appraisal of tight sandstones of upper Triassic Xujiahe formation in the western Sichuan foreland basin," *Natural Gas Geosciences*, vol. 17, pp. 456–462, 2006.

[17] M. Nobakht and C. R. Clarkson, "Analysis of production data in shale gas reservoirs: rigorous corrections for fluid and flow properties," in *SPE Eastern Regional Meeting*, pp. 85–98, Columbus, Ohio, USA, 2011.

[18] R. Christopher, J. L. Clarkson, P. K. Jensen, and M. F. Pedersen, "Innovative methods for flow-unit and pore-structure analyses in a tight siltstone and shale gas reservoir," *AAPG Bulletin*, vol. 96, no. 2, pp. 355–374, 2012.

[19] Z. Y. Gao, Y. P. Fan, Q. X. Xuan, and G. W. Zheng, "A review of shale pore structure evolution characteristics with increasing thermal maturities," *Advances in Geo-Energy Research*, vol. 4, no. 3, pp. 247–259, 2020.

[20] Y. Li, X. Gao, S. Meng, P. Wu, and D. Elsworth, "Diagenetic sequences of continuously deposited tight sandstones in various environments: a case study from Upper Paleozoic sandstones in the Linxing area, eastern Ordos basin, China," *AAPG Bulletin*, vol. 103, no. 11, pp. 2757–2783, 2019.

[21] Y. Li, J. Yang, Z. Pan, S. Meng, K. Wang, and X. Niu, "Unconventional natural gas accumulations in stacked deposits: a discussion of Upper Paleozoic coal-bearing strata in the east margin of the Ordos basin, China," *Bulletin of the Geological Society of China*, vol. 93, no. 1, pp. 111–129, 2019.

[22] Y. Li, W. Xu, P. Wu, and S. Meng, "Dissolution versus cementation and its role in determining tight sandstone quality: a case study from the Upper Paleozoic in northeastern Ordos basin, China," *Journal of Natural Gas Science and Engineering*, vol. 78, 2020.

[23] H. Deng, R. Leguizamon, and R. Aguilera, "Petrophysics of triple porosity tight gas reservoirs with a link to gas productivity," *SPE Reservoir Evaluation & Engineering*, vol. 14, no. 5, pp. 566–577, 2011.

[24] J. Lai, G. Wang, Z. Fan et al., "Fracture detection in oil-based drilling mud using a combination of borehole image and sonic logs," *Marine and Petroleum Geology*, vol. 84, pp. 195–214, 2017.

[25] S. P. Chen, L. J. Tang, Z. J. Jin, C. Z. Jia, and X. J. Pi, "Thrust and fold tectonics and the role of evaporites in deformation in the Western Kuqa Foreland of Tarim Basin, Northwest China," *Marine and Petroleum Geology*, vol. 21, no. 8, pp. 1027–1042, 2004.

[26] X. F. Fu, Y. Song, Y. F. Lü, and Y. H. Sun, "Rock mechanic characteristic of gypsum cover and conservation function to gas in the Kuche Depression, the Tarim Basin," *Petroleum Geology & Experiment*, vol. 28, pp. 25–29, 2006.

[27] P. L. Li, *Tectonic Sedimentary and Accumulation in Tarim Basin*, Geological Publishing House, Beijing, 2010.

[28] S. Q. Li, L. Feng, P. C. Tang, G. Rao, and Y. Bao, "Calculation of depth to detachment and its significance in the Kuqa Depression: a discussion," *Petroleum Science*, vol. 6, no. 1, pp. 17–20, 2009.

[29] J. Lai, G. Wang, S. Wang et al., "A review on the applications of image logs in structural analysis and sedimentary characterization," *Marine and Petroleum Geology*, vol. 95, pp. 139–166, 2018.

[30] J. Lai, D. Li, G. Wang et al., "Earth stress and reservoir quality evaluation in high and steep structure: the Lower Cretaceous in the Kuqa Depression, Tarim Basin, China," *Marine and Petroleum Geology*, vol. 101, pp. 43–54, 2019.

[31] D. F. He, X. Y. Zhou, H. J. Yang, G. L. Lei, and Y. J. Ma, "Geological structure and its controls on giant oil and gas fields in Kuqa Depression, Tarim Basin: a clue from new shot seismic data," *Geotectonica et Metallogenia*, vol. 33, pp. 19–32, 2009.

[32] C. Z. Jia, H. L. Chen, S. F. Yang, H. F. Lu, and Y. Z. Zhou, "Late Cretaceous uplifting process and its geological response in Kuqa Depression," *Acta Petroleum Sinica*, vol. 24, pp. 1–5, 2003.

[33] X. Wang, C. Z. Jia, and S. F. Yang, "Geometry and kinematics of the Kuqa fold-and-thrust belt in the southern Tianshan," *Chinese Journal of Geology*, vol. 37, pp. 372–384, 2002.

[34] J. Lai, G. Wang, Y. Chai et al., "Deep burial diagenesis and reservoir quality evolution of high-temperature, high-pressure sandstones: examples from Lower Cretaceous Bashijiqike Formation in Keshen area, Kuqa Depression, Tarim Basin of China," *AAPG Bulletin*, vol. 101, no. 6, pp. 829–862, 2017.

[35] T. Nian, G. Wang, C. Xiao, L. Zhou, L. Deng, and R. Li, "The in situ stress determination from borehole image logs in the Kuqa Depression," *Journal of Natural Gas Science and Engineering*, vol. 34, pp. 1077–1084, 2016.

[36] T. Nian, Z. Jiang, G. Wang et al., "Characterization of braided river-delta facies in the Tarim Basin Lower Cretaceous: application of borehole image logs with comparative outcrops and cores," *Marine and Petroleum Geology*, vol. 97, pp. 1–23, 2018.

[37] Z. Gao, H. Guo, R. Zhu, L. Zhang, and Y. Sun, "Sedimentary response of different fan types to the Paleogene–Neogene Basin transformation in the Kuqa Depression, Tarim Basin, Xinjiang Province," *Acta Geologica Sinica*, vol. 83, no. 2, pp. 411–424, 2009.

[38] Z. Li, D. X. Wang, and W. Lin, "Mesozoic-Cenozoic elastic composition in Kuqa Depression, northwest China: implication for provenance types and tectonic attributes," *Acta Petrologica Sinica*, vol. 20, pp. 655–661, 2004.

[39] C. S. Lin, J. Y. Liu, Y. M. Zhang, J. Xiao, J. Chen, and Y. Ji, "Depositional architecture of the Tertiary tectonic sequences and their response to foreland tectonism in the Kuqa Depression, the Tarim Basin," *Science*, vol. 45, no. 3, pp. 250–258, 2002.

[40] Y. Q. Jiang, L. Chen, C. Jiang et al., "Characterization techniques and trends of the pore structure of tight reservoirs," *Geological Science and Technology Information*, vol. 33, pp. 63–70, 2014.

[41] X. D. Sun, L. M. Suo, M. Z. Zhang, and P. J. Wang, "New progress of reservoir research by the technology of laser confocal scanning microscope analysis in the Daqing exploration area," *Acta Petrologica Sinica*, vol. 21, pp. 1479–1488, 2005.

[42] H. Gao, W. Xie, and J. P. Yang, "Pore throat characteristics of extra-ultra low permeability sandstone reservoir based on constant-rate mercury penetration technique," *Petroleum Geology & Experiment*, vol. 33, pp. 206–214, 2011.

[43] Y. L. Gao and Z. G. Zhang, "Valuation on difference of pore throat structure of low permeability sandstone by constant mercury penetration technique," *Geological Science and Technology Information*, vol. 30, pp. 73–76, 2011.

[44] G. R. L. Chalmers and R. Marc Bustin, "On the effects of petrographic composition on coalbed methane sorption," *International Journal of Coal Geology*, vol. 69, no. 4, pp. 288–304, 2007.

[45] D. Prinz and R. Littke, "Development of the micro- and ultra-microporous structure of coals with rank as deduced from the accessibility to water," *Fuel*, vol. 84, pp. 1645–1652, 2005.

[46] N. H. Kilmer, N. R. Morrow, and J. K. Pitman, "Pressure sensitivity of low permeability sandstones," *Journal of Petroleum Science and Engineering*, vol. 1, no. 1, pp. 65–81, 1987.

[47] R. G. Loucks, R. M. Reed, S. C. Ruppel, and D. M. Jarvie, "Morphology, genesis, and distribution of nanometer-scale pores in siliceous mudstones of the Mississippian Barnett shale," *Journal of Sedimentary Research*, vol. 79, no. 12, pp. 848–861, 2009.

[48] L. M. Ma, C. Y. Lin, and M. W. Fan, "Quantitative classification and evaluation of reservoir based on fractal features of micro-pore structures," *Journal of Oil and Gas Technology*, vol. 34, pp. 15–19, 2012.

[49] T. Zhang, S. Y. Xu, and K. Yang, "Application of fractal dimension of micro pore structure," *Journal of Daqing Petroleum Institute*, vol. 34, pp. 44–47, 2010.

[50] G. S. He, *Reservoir Physics*, Petroleum Industry Press, Beijing, 1993.

[51] A. Salah, "The impact of pore geometry aspects on porosity-permeability relationship-a critical review to evaluate NMR estimated permeability," in *Paper presented at the North Africa Technical Conference and Exhibition*, Cairo, Egypt, 2012.

[52] X. C. Wang, Y. R. Fan, S. G. Deng, K. Z. Li, Z. Q. Li, and J. L. Jiang, "Irreducible water saturation determination based on centrifugal test data," *Journal of China University of Petroleum*, vol. 33, pp. 76–79, 2009.

[53] Y. Xiang, D. Xiang, and Y. C. Yang, "Study of gas recovery and water film thickness in water drive for tight sandstone gas reservoir," *Journal of Chengdu University of Technology Science and Technology Edition*, vol. 26, pp. 389–391, 1999.